
Taylor & Francis
Taylor & Francis Group

Applied Earth Science

Transactions of the Institutions of Mining and Metallurgy

ISSN: (Print) (Online) Journal homepage: https://www.tandfonline.com/loi/yaes21

# Compositional characteristics of mineralised and unmineralised gneisses and schist around the Abansuoso area, southwestern Ghana

**Raymond Webrah Kazapoe, Olugbenga Okunlola, Emmanuel Arhin, Olusegun Olisa, Daniel Kwayisi, Elikplim Abla Dzikunoo & Ebenezer Ebo Yahans Amuah**

**To cite this article:** Raymond Webrah Kazapoe, Olugbenga Okunlola, Emmanuel Arhin, Olusegun Olisa, Daniel Kwayisi, Elikplim Abla Dzikunoo & Ebenezer Ebo Yahans Amuah (2023) Compositional characteristics of mineralised and unmineralised gneisses and schist around the Abansuoso area, southwestern Ghana, Applied Earth Science, 132:1, 36-51, DOI: 10.1080/25726838.2023.2166725

**To link to this article:** https://doi.org/10.1080/25726838.2023.2166725

Published online: 23 Jan 2023.

APPLIED EARTH SCIENCE (TRANS. INST. MIN. METALL. B)
2023, VOL. 132, NO. 1, 36–51
https://doi.org/10.1080/25726838.2023.2166725

I·M3 Institute of Materials, Minerals & Mining
AusIMM THE MINERALS INSTITUTE
Taylor & Francis Taylor & Francis Group

RESEARCH ARTICLE



# Compositional characteristics of mineralised and unmineralised gneisses and schist around the Abansuoso area, southwestern Ghana

Raymond Webrah Kazapoe [a,c], Olugbenga Okunlola [b,c], Emmanuel Arhin [d], Olusegun Olisa [e], Daniel Kwayisi [f], Elikplim Abla Dzikunoo [f] and Ebenezer Ebo Yahans Amuah [g]

[a]Department of Geological Engineering, University for Development Studies, Nyankpala, Ghana; [b]Department of Geology, University of Ibadan, Ibadan, Nigeria; [c]Pan African University Life and Earth Sciences Institute (PAULESI), University of Ibadan, Ibadan, Nigeria; [d]Department of Geological Sciences, University of Energy and Natural Resources, Sunyani, Ghana; [e]Departement of Earth Science, Olabisi Onabanjo University, Ago-Iwoye, Nigeria; [f]Earth Science Department, University of Ghana, Accra, Ghana; [g]Environmental Science Department, Kwame Nkrumah University of Science and Technology, Kumasi, Ghana

**ABSTRACT**

Gold-bearing granitoid deposits have recently been discovered in the Birimian of Ghana but their mode of formation and ore genesis remain enigmatic. This study presents petrographic, and geochemical characteristics of mineralised and unmineralised (gold grade >0.05 and <0.05 g/t respectively) granitoids (now gneisses) and schists (metasedimentary) to evaluate their petrogenesis/provenance, and relationship to gold mineralisation in the Abansuoso area. The unmineralised rocks comprise biotite- and hornblende-biotite gneisses, sericite-quartz, carbonate-sericite, and biotite-quartz schist. The mineralised varieties are biotite-, muscovite gneiss, iron-carbonate-sericite, carbonate-sericite-quartz, chlorite-carbonate, and biotite-carbonate schist. The mineralised and unmineralised gneisses are both metaluminous and peraluminous. Both mineralised and unmineraised gneiss and schist show Nb-Ta trough, depleted LILE and enriched HFSE although widespread overall trace element concentrations for the mineralised rocks on UCC-normalised multi-element diagram, suggestive of their formation in an arc setting. This suggests coeval granitic plutonism and sedimentation with subduction-accretion during the Eburnean orogeny, hence, mineralisation may be orogenic-type.

**ARTICLE HISTORY**
Received 19 August 2022
Revised 4 January 2023
Accepted 4 January 2023

**KEYWORDS**
Geochemistry; gold mineralisation; gold exploration; Ghana; petrology

## Introduction

Gold exploration in the Paleoproterozoic Birimian has primarily focused on sediment-hosted shear zones, lode-quartz veins, disseminated sulphides, and auriferous quartz-pebble conglomerates where large deposits have formed the basis of gold extraction (e.g. Smith et al. 2016; Agbenyezi et al. 2020). In recent years, gold resources in the Birimian granitoid have become viable targets for exploration in an effort to maximise the gold ore resource base and boost productivity (Amponsah et al. 2016; Bouabdellah and Slack 2016; Takyi-Kyeremeh et al. 2019). The Chirano, Nhyiaso, Ayanfuri, and Ayankyerim gold deposits in the western portion of the Sefwi and Ashanti Belts are discussed as prime examples of gold-bearing granitoid bodies (Allibone et al. 2004; Fougerouse et al. 2017).

However, understanding of the geological characteristics of granitoid gold deposits in Ghana is limited (Griffis et al., 2002). Owing to similarities in wall-rock alteration, elemental associations, structural controls, and ore fluids (Goldfarb et al. 2001; Groves et al. 2003), the distinctions between orogenic gold-bearing granitoids and intrusion-related gold deposits continue to be debated (Sillitoe 1991 Agbenyezi et al. 2020). Consequently, several gold-bearing granitoids, such as the True North deposit (Canada) and the Muruntau gold deposits (Uzbekishas), have been described as both intrusion-related and orogenic deposits (Kempe et al. 2001; Hart et al. 2002). Given the numerous gold exploration techniques associated with intrusion-related and orogenic gold classifications, it is essential to identify each model accurately (Goldfarb et al. 2005).

The tectonothermal Eburnean orogeny that occurred between 2120 and 2080 Ma coincides with the placement of granitoid plutons within the Paleoproterozoic Birimian terrane (Oberthür et al. 1998). (Oberthür et al. 1998). This study examined auriferous granitoid bodies (now gneisses) and associated sedimentary rocks (now schist) from the Abansuaso area in the Sefwi-Bibiani greenstone belt in order to gain a better understanding of the nature and genesis of the granitoid and its associated gold mineralisation (orogenic-bearing vs. intrusive-related) for improved modelling and exploration in the study area. The whole-rock major and trace element compositions of mineralised and unmineralised rocks are compared in order to evaluate their petrogenesis and tectonic

**CONTACT** Raymond Webrah Kazapoe rkazapoe@yahoo.com Department of Geological Engineering, School of Engineering, University for Development Studies, P.O. Box TL 1350, Tamale, Ghana

setting and assess their relationship to gold mineralisation within the deposit.

## Geology of the Abansuoso deposit

The study area lies within one of Ghana's six known Birimian Greenstone Gold Belts, the Sefwi-Bibiani Greenstone Belt (Figure 1). There are varying degrees of gold mineralisation in the vicinity of these belts (Perrouty et al. 2012). Two of the six Greenstone Gold Belts are home to the most productive mines, while the remaining four have been subject to advanced exploration and modest mining. In the Sefwi-Bibiani Greenstone Gold Belt, gold mining and prospecting have a rich history. The Belt contains some of the most renowned mines, such as the Chirano, Kenyasi, and Bibiani mines (Griffis et al. 2002; Kazapoe et al. 2021). On the Belt, there are a few small to medium-sized businesses whose exploration and mining operations are in varying stages of development and success (Griffis et al. 2002). Subriso-Nfante is the location of the research area in the Ahafoano North District of the city of Ahafoano.

The Sefwi-Bibiani Greenstone Gold Belt is situated northwest of the Ashanti Greenstone Gold Belt and is underlain by metavolcanic and metasedimentary rocks that are granitoids and mafic units (Galipp et al. 2003; Senyah et al. 2016). The majority of the metavolcanic rocks are massive and pillow basalts, basaltic andesite, dacites, and rhyolites with tholeiitic to calc-alkaline signatures (Perrouty et al. 2012; Senyah et al. 2016). The majority of the metasedimentary rocks consist of phyllites, wackes, and a volcaniclastic unit with pyroclastics and epiclastics (Jessell et al. 2012; Perrouty et al. 2012). The metavolcanics and metasedimentary rocks are intruded by syn-volcanic tonalitic to granodioritic granitoids (Jessell et al. 2012). These granitoids have now been metamorphosed into various gneisses (Kazapoe et al. 2022). The Sunyani Basin is bordered to the west by the Sefwi-Bibiani Greenstone Gold Belt and to the east by the Kumasi Basin (Griffis and Agezo 2000).

### *Sampling and analytical methodology*

Twenty-three rock samples were sent to ALS geochemical laboratory in Vancouver for whole-rock major and minor elements, and trace elements composition. The rocks were taken from the mineralised zone (14 samples), and the unmineralised zone (9 samples). In this study, the mineralised and unmineralised samples are classified based on gold grade. Samples with gold grade above 0.05 g/t are considered mineralised whiles samples with gold grade below 0.05 g/t are considered as unmineralised. Whole-rock major element analysis was carried out using ICP-AES. Loss on Ignition (LOI) at 1000°C was determined using a thermo gravimetric analyser (TGA). Forty-one selected minor and trace elements were analysed. Thirty-one minor and trace elements were analysed using lithium borate fusion ICP-MS. Concentrations of the other ten elements (Ag, Co, Ni, Zn, As, Cu, Pb, Cd, Mo, and Sc) were obtained by ICP-AES from a separate four-acid digestion following standard procedure. Precisions is better than 5%. For elements present in significant concentrations (>1 wt. %.) and elements in low concentrations (<1 wt. %), analytical uncertainties were 1–3% and ≈10% respectively.

## Petrography

As mentioned above, the rocks of the study area can be grouped into two: these are mineralised (with >0.05 g/t) and unmineralised (with <0.05 g/t) varieties. From petrographic investigations, both the mineralised and unmineralised varieties are made up of gneisses (metagranitoids) and schists (metasedimentary rocks).

### *Unmineralised rocks*

#### *Gneisses*

The unmineralised gneisses are of two varieties based on mineralogical composition. These are the Biotite gneiss and Hornblende-Biotite gneiss. Generally, the gneisses are medium-grained and are weakly to strongly foliated. The biotite-gneiss is composed of quartz, plagioclase, microcline, and biotite (Figure 2(a)). Cubic to slightly elongated sulphide minerals can be observed. The biotite and elongated opaque minerals define the foliation and mineral elongation (Figure 2(a)). Quartz is anhedral, exhibits undulose extinction, appears recrystallised, and occurs as either coarse crystals or medium-grained, elongated aggregates. Plagioclase and microcline are subhedral to anhedral and weakly altered to sericite. The biotite shows very weak alterations mostly into chlorite. The hornblende-biotite gneiss is foliated with compositional banding of felsic bands alternating with mafic bands. In general, this rock is composed of hornblende, biotite, garnet, plagioclase, quartz, and microcline (Figure 2(b)). The first three minerals comprise the mafic bands whereas the latter three comprise the felsic bands. The mineral assemblage is structurally competent although individual grains are slightly elongated, broken, or cracked. The garnet and microcline in some samples are very coarse and poikilitic with inclusions of quartz and occasional biotite (Figure 2(b,c)). Associated with the garnet and often occurring within the foliation are subhedral to cubic opaque sulphide minerals. Hornblende has partially altered to epidote whereas the feldspars and biotite have partially altered to sericite and chlorite,

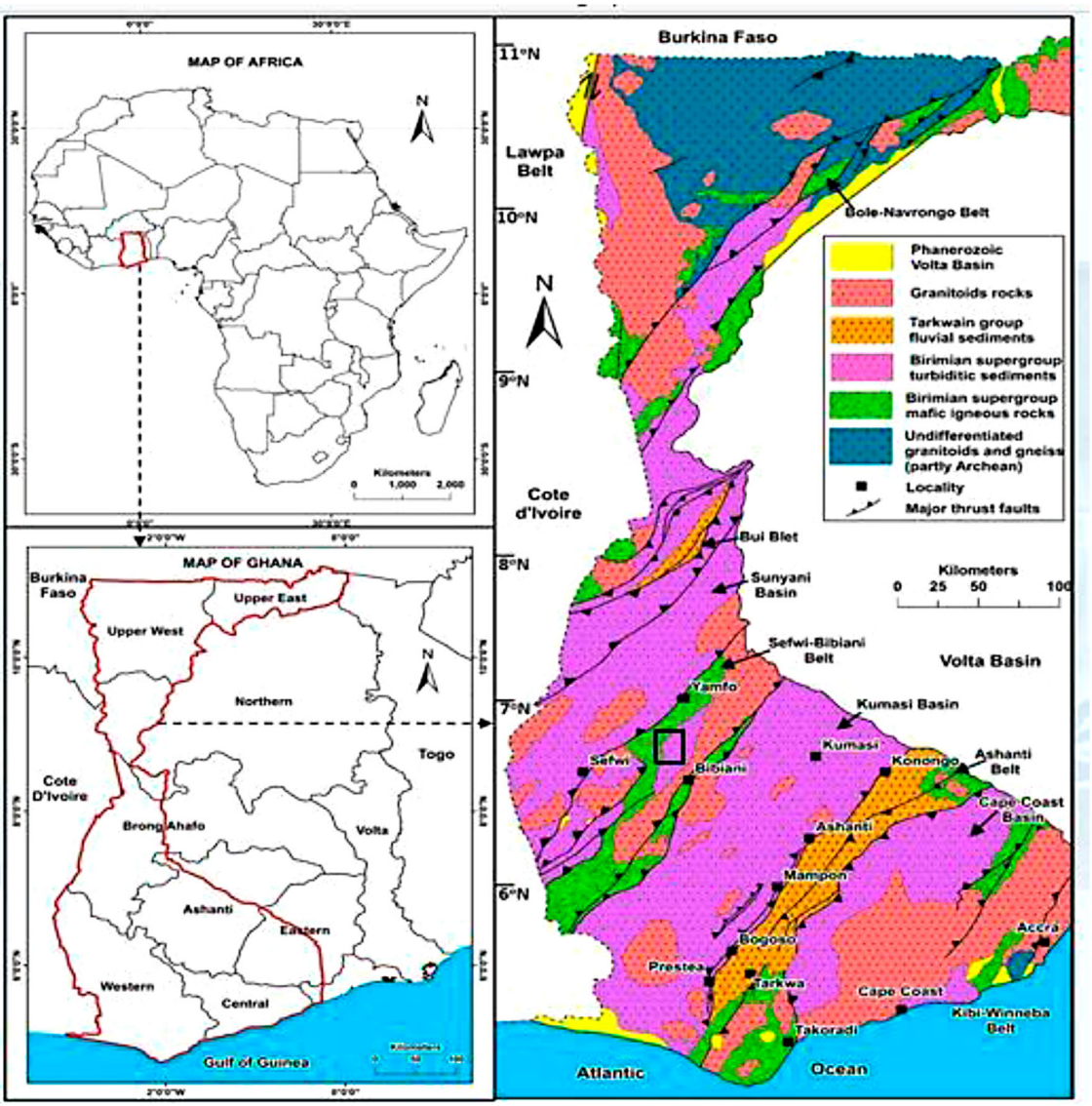


**Figure 1.** Geological map of the study area.

respectively. Quartz is elongated and exhibits undulose extinction.

### *Schist*

The schist is surrounded by the gneisses and appear weathered across the area. The schists are of three types: the carbonate-sericite, sericite-quartz, and biotite-quartz schist. The carbonate-sericite schist is medium-grained and weakly foliated. It is composed of quartz, plagioclase, sericite, and carbonate (calcite) (Figure 2(d)). The calcite is very coarse in the veins and also has few impregnations. Quartz is recrystallised grains, maybe associated with the carbonate or as impregnations. The sericite-quartz schist is medium-grained and composed mainly of sericite, and quartz (Figure 2(e)). Fine to medium-grained texture and strong foliation characterise the biotite-quartz schist (Figure 2(f)). This rock is dominantly composed of quartz and biotite together with minor feldspar. Rare occurrence of disseminated cubic sulphide minerals can be observed in the rocks. The rock is cut by quartz vein composed of coarse-grained quartz mineral.

### *Quartz veins*

Three main generations of quartz veins (types A, B, and C) within the pits and mine sites have been identified which were corroborated with the measurements taken from the drill core. All veins are unmineralised. Type A can be observed as NNE-SSW veins associated with pegmatite within the shear zone. Type B is NE-SW with Type C observed in the mining pits as upright E-W which can measure several metres in width and appear heavily weathered (Figure 3(a,b)).

Petrographically, the quartz veins are very coarse-grained and composed mainly of quartz. In few samples the quartz is slightly sheared (Figure 4(a)). The quartz grains show undulose extinction, some however, exhibit chessboard extinction (Figure 4(b)). In some samples, the quartz is elongated.

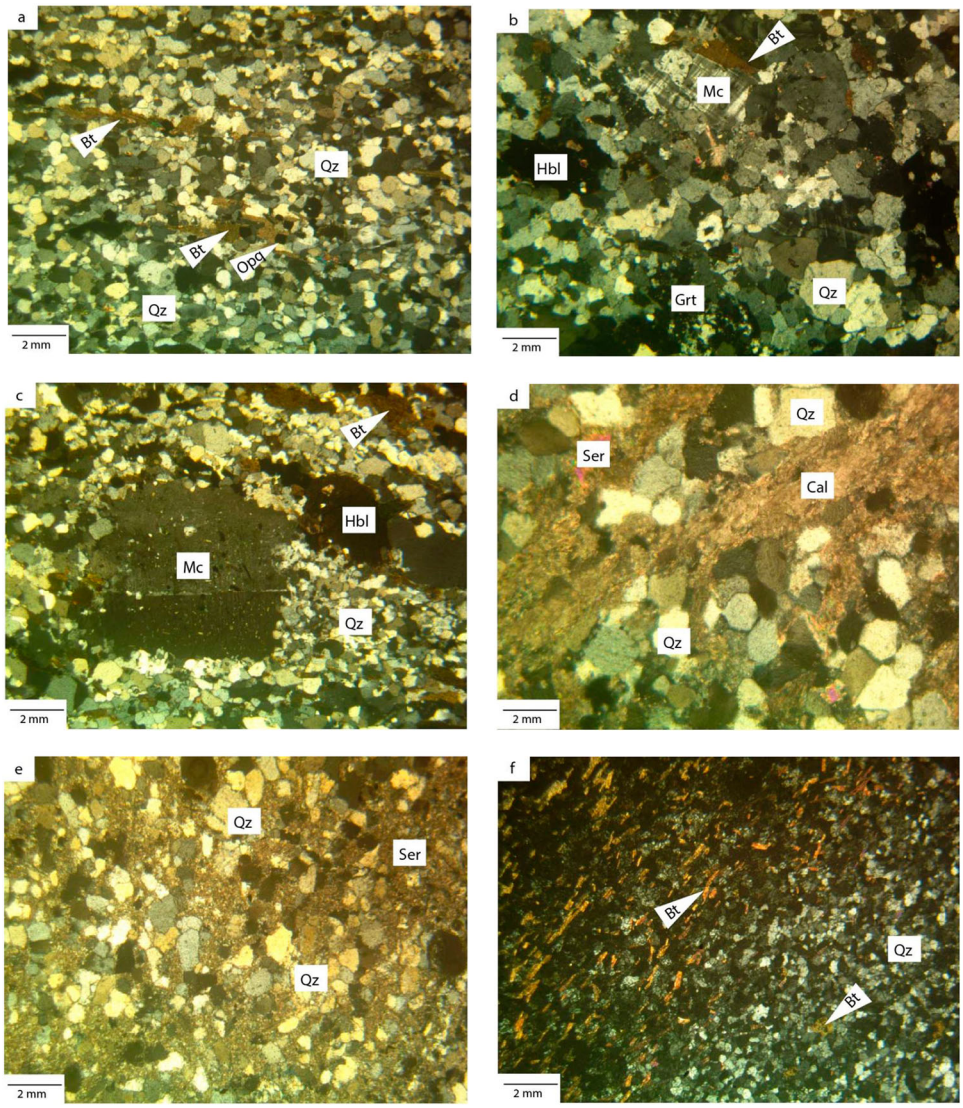


**Figure 2.** (a) Photomicrographs of biotite gneiss with strong foliation (b) Photomicrographs of hornblende-biotite gneiss (c) Photomicrographs of hornblende-biotite gneiss with coarse microcline showing inclusions of quartz (d) Photomicrographs of carbonate-sericite schist (e) Photomicrographs of sericite-quartz schist (f) Photomicrographs of muscovite-quartz schist. Mineral abbreviations: Mc = Microcline, Bt = Biotite, Qz = Quartz, Ser = Sericite, Cal = Calcite, Hbl = Hornblende (Whitney and Evans, 2010).

(a) (b)

**Figure 3.** (a) Field photograph of type C quartz vein observed in the mining pits near Subriso (b) Field photograph of type B quartz vein encountered near the Nfante township (picture taken facing NE).

### Mineralised (host) rocks

The rocks hosting the gold mineralisation in the Abansuoso deposit are strongly sheared metamorphosed biotite gneiss, muscovite gneiss, and schists. Gold mineralisation is not visible on the outcrop, as the area is entirely covered with a thick lateritic cover at least 10 m in width, which overlies a saprolite horizon that extends further down.

Based on mineralogical and textural characteristics, the mineralised schist can be grouped into four. These are iron-carbonate-sericite schist, carbonate-sericite-quartz schist, chlorite-carbonate schist, and biotite-carbonate schist (Figure 5(a–f)). Fine to medium grains characterised the biotite-carbonate (calcite) schist (Figure 5(a)). This type of schist has undergone significant alteration expressed as chlorite from the biotite and carbonate infiltration. The rock is strongly foliated, with the mineral assemblage slightly elongated. The carbonate (calcite)-sericite-quartz schist is medium-grained and strongly foliated. It is composed of quartz, Plagioclase, K-feldspar, and sulphides embedded in a network of sericite-carbonate matrix (Figure 5(b)). This mineral assemblage is elongated as a result of shearing and in some samples infiltrated with interstitial calcitic stringers.

The opaque minerals are sulphides and occur as isolated grains intersperse in the carbonate-sericite matrix (Figure 5(b)). Sulphides at portions of the thin section are slightly elongated. Quartz is deformed with undulose extinction. The feldspars appear weakly altered to sericite. The carbonate, quartz and sericite composition vary. Some samples have more carbonate-sericite than quartz (Figure 5 (c)). On the other hand, some samples have more quartz than carbonate-sericite (Figure 5(d)). The iron-carbonate (ankarite) -sericite schist is medium to coarse-grained, strongly foliated with elongated grains. It is composed of iron, carbonate, sericite, quartz, sulphide, plagioclase, and chlorite (Figure 5 (e)). Network of iron-carbonate veins cut this rock. The chlorite-carbonate (calcite) schist in thin section is fine-grained, weakly foliated, and composed of chlorite, sericitised plagioclase and abundant opaque minerals (Figure 5(f)). The assemblage is cut by thin quartz-calcite veinlet. The calcites are relatively coarse and recrystallised.

The mineralised biotite gneiss is coarse-grained and foliated. It is composed primarily of quartz, plagioclase, microcline, and biotite with carbonate and sulphide minerals being secondary (Figure 6(a,b)). The mineral assemblage is slightly altered and deformed with quartz cracked and undulose, and plagioclase and biotite altered to sericite and chlorite, respectively. The opaque minerals are the result of alteration of formal ferromagnesian minerals and sulphide. The carbonate occurs as later infiltrations in the microcline and interstitial and defines the foliation. The muscovite gneiss is medium to coarse-grained and foliated (Figure 6(c)). It is composed of quartz, plagioclase, muscovite, and carbonate. This assemblage defines foliation and mineral elongation. Quartz is anhedral, exhibits undulose extinction, appears recrystallised, and occurs as either coarse crystals or medium-grained, elongated aggregates. Plagioclase is subhedral to anhedral and maybe weakly altered. The muscovite is significantly shredded into sericite.

## Geochemistry

### Major and trace elements characteristics

#### Gneiss

The major and trace element concentrations of the gneisses are presented in Table 1. The mineralised gneiss has lower $SiO_2$ contents of average 66.8 wt. % than the mineralised gneiss with average $SiO_2$ contents of 76.9 wt.%. The unmineralised gneiss on average has higher $Na_2O$ (3.79wt. %), and $K_2O$ (2.98 wt. %) than the mineralised gneiss ($Na_2O$ = 3.10 wt. %, $K_2O$ = 2.00 wt.%). However, FeOt, MgO, and CaO are higher in the mineralised gneiss than the unmineralised gneiss. On the Al saturation diagram after Shand (1948), the mineralised gneiss shows A/CNK values typical of metaluminous with only one sample being peraluminous (Figure 7(a)). The unmineralised gneiss, however, have A/CNK values comparable to both metaluminous and peraluminous rocks (Figure 7(a)). The total alkalis vs silica diagram show that the gneiss is mainly granite (Figure 7(b)). Only one sample of the mineralised gneiss plots on the boundary line between monzodiorite and gabbroic diorite. On the normative feldspar discrimination plots after Barker (1979) the unmineralised gneiss plot mostly as granite with the mineralised gneiss plotting as trondhjemite (Figure 7(c)).

On the chondrite normalised REE diagram, both the mineralised and unmineralised gneisses display enriched LREE and nearly flat HREE patterns (Figure 8(a,b)). However, the mineralised gneiss shows a wide range of REE concentrations than the unmineralised gneiss (Figure 8(c,d)). On the multi-elements normalised to the UCC diagram, the gneisses show the depleted concentration of LILE and enriched contents of HFSE including the HREE (La/Yb = 1.73–3.52) (unmineralised) and La/Yb = 2.79–7.44 (mineralised). The unmineralised gneiss displays a typical Nb-Ta trough, negative U, Th, Sr, P, and Ti peaks (Figure 8(a)). The mineralised gneiss has negative Th, Nb-Ta, and Ti peaks (Figure 8(b)).

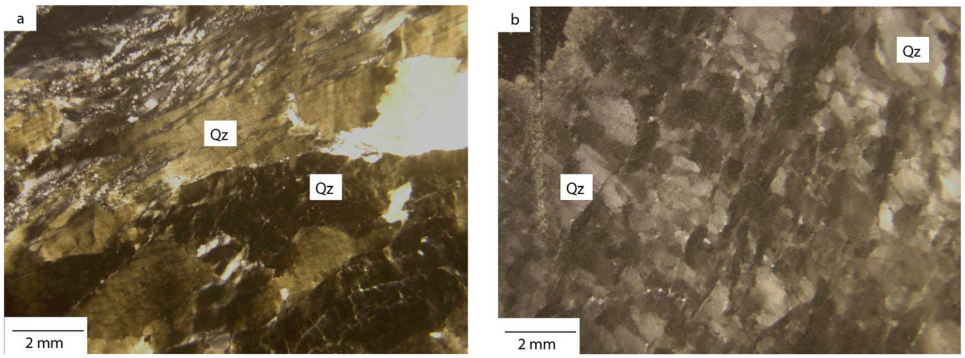


**Figure 4.** (a) Photomicrographs of quartz showing strong elongation and pressure shadow (b) Photomicrographs of quartz showing chess board extinction.

### *Schists*

Table 2 presents the whole-rock major and trace element concentrations of the schists of the study area. The mineralised schist has on average lower $SiO_2$ content ($SiO_2$ = avg. 63 wt.%) than the unmineralised schist ($SiO_2$ = avg. 70 wt.%). MgO, FeOt, CaO,

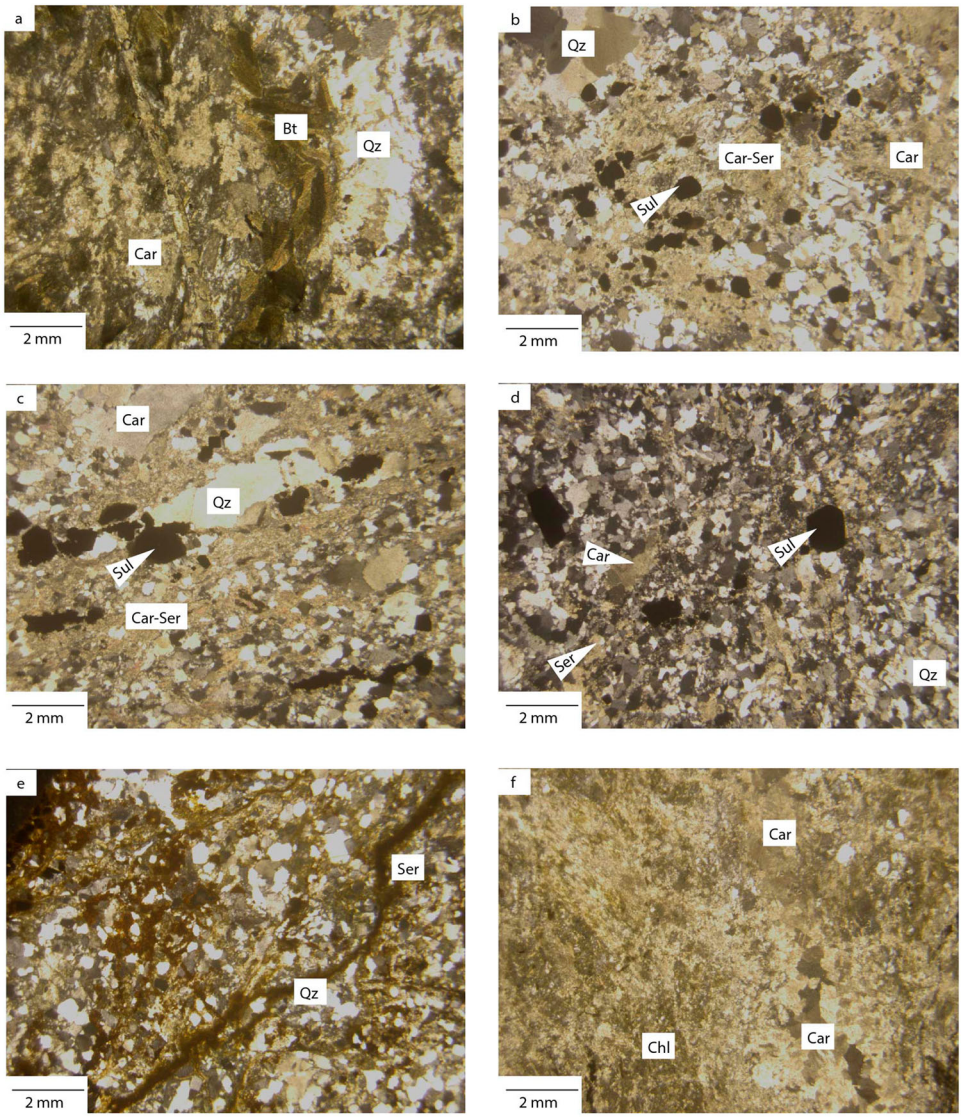


**Figure 5.** (a) Photomicrographs of biotite-carbonate schist with strong foliation (b) Photomicrographs of carbonate-sericite-quartz schists showing sub-cubic sulphides intersperse in carbonated-sericite matrix (c) Photomicrographs of carbonate-sericite-quartz schist with abundant carbonate-sericite content than quartz (d) Photomicrographs of carbonate-sericite-quartz schist with abundant quartz than carbonate-sericite (e) Photomicrographs of iron-carbonate schist (f) Photomicrographs of chlorite-carbonate schist. Mineral abbreviations: Ser = Sericite, Car = Carbonate, Qz = Quartz, Sul = Sulphide, Chl = Chlorite, Bt = Biotite, from Whitney and Evans, 2010.

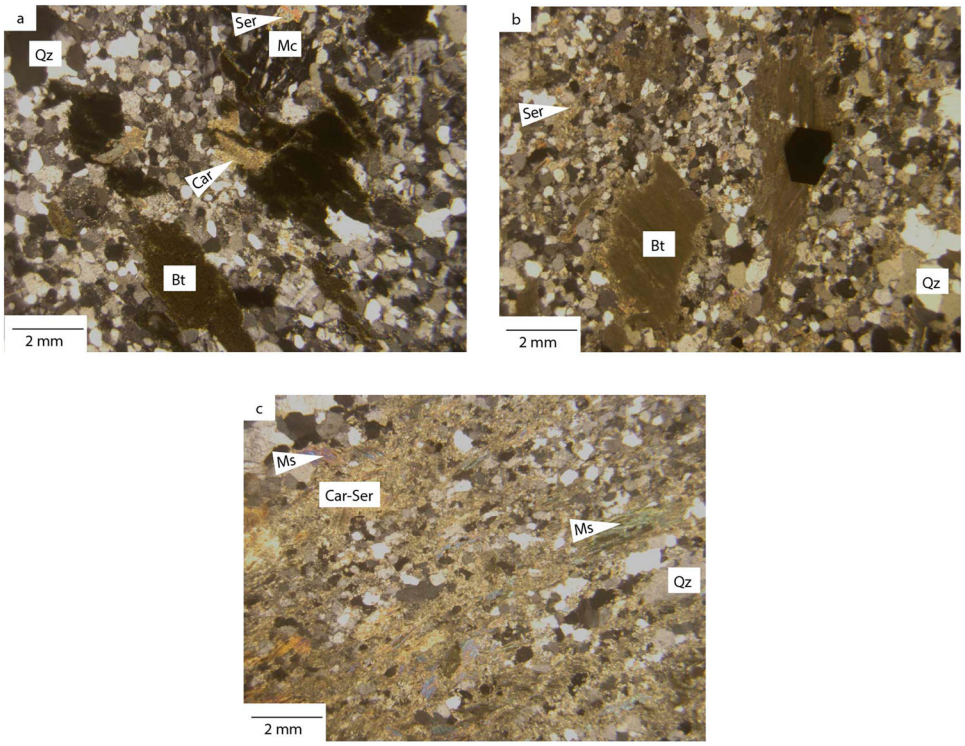


**Figure 6.** (a) Photomicrographs of biotite-rich granitoid gneiss showing biotite-microcline-quartz-carbonate assemblage (b) Photomicrographs of biotite-rich granitoid gneiss showing cubic sulphide mineralisation (c) Photomicrographs of biotite-rich granitoid gneiss showing muscovite gneiss.

and $Na_2O$ contents are on average higher in the mineralised schist than in the unmineralised schist. $K_2O$ content is similar in both mineralised and unmineralised schists. The schists have low $SiO_2/Al_3O_2$ between 4.1 and 7.2. On the chondrite normalised REE diagram the schists define almost similar patterns with enriched LREE, nearly flat HREE (La/Yb = 3.03–4.23 (unmineralised schist) and La/Yb = 2.87–3.95 (mineralised schist)) and pronounced Eu negative anomalies (Figure 9(a,b)). The REE patterns defined by the schist are comparable to Upper Continental Crust (UCC) and Post-Archean Australian Shale (PAAS) (Figure 9(a,b)).

On the multi-elements normalised to UCC diagram (Figure 9(c,d)), the schists show depleted concentration of LILE and enriched contents of HFSE including the HREE. Although the mineralised and unmineralised schists show similar patterns, the mineralised exhibits slightly more widespread multi-element concentrations than the unmineralised ones. Besides, the mineralised depict positive peaks of K, Sr, and Ti (although Ti in some samples show negative peak) and negative peaks of Nb-Ta (8d). The unmineralised on other hand, have negative Nb-Ta, Sr, and Ti peaks (Figure 8(c)).

## Discussion

### *Mineralisation*

The concession lies within a ductile sinistral shear zone with a brittle component. The mineralisation appears to sit on a granitoid pluton (now gneisses of felsic to intermediate composition) and arenaceous-argillaceous sedimentary rocks (now schist of varying compositions) which have been affected by various stages of metamorphism and deformation. The sequence of alteration invades the rocks via stringers along weak zones probably caused by the shearing. The alteration is predominantly quartz-sericite, carbonate, sulphides (pyrite, arsenopyrite, and galena) with haematite at the fringes where low grade gold is reported. The main mineralised zones are characterised by sericite alteration coupled with fine-grain pyrite and associated with carbonates. The preliminary sequence of alteration has been deduced as chlorite-carbonate-haematite-sericite-chlorite -silica/sulphides with minor albite.

### *Influence of alteration and metamorphism on the composition of the rocks*

Therefore, it is important to evaluate the influence of metamorphism on the mobility of the major and trace elements in the rocks. During metamorphism, some elements, such as Cs, Rb, K, Na, Ca, Sr, and Ba are mobilised (Schiano et al. 1993) and thus increasing the LOI content of the rock. The gneiss samples have low LOI content (0.5–4.0 wt.%), except one mineralised gneiss with very high LOI content of 18.1 wt. % (Table 1), which makes it less likely that significant remobilisation of these major elements has occurred

**Table 1.** Major and trace elements composition of the gneiss.

| | Unmineralised Gneiss | | | | Mineralised Gneiss | | | |
|---|---|---|---|---|---|---|---|---|
| Sample | 021/KOS | 013/N | 027/KS | 020/KOS | 016/79 | 017/79 | 018/79 | 040/PK |
| $SiO_2$ | 76.9 | 73 | 75.9 | 78.9 | 41.9 | 80.8 | 74.1 | 70.5 |
| $TiO_2$ | 0.23 | 0.37 | 0.19 | 0.24 | 0.43 | 0.28 | 0.33 | 0.49 |
| $Al_2O_3$ | 11.35 | 11.6 | 11.4 | 12 | 11.2 | 8.91 | 11.55 | 11.4 |
| FeOt | 3.01 | 5.9 | 3.01 | 1.67 | 6.23 | 2.37 | 2.96 | 5.68 |
| MnO | 0.03 | 0.13 | 0.1 | 0.02 | 0.18 | 0.06 | 0.06 | 0.13 |
| MgO | 0.18 | 0.24 | 0.54 | 0.24 | 5.97 | 0.48 | 0.56 | 0.55 |
| CaO | 0.43 | 1.87 | 1.83 | 0.71 | 9.62 | 1.4 | 1.34 | 1.04 |
| $Na_2O$ | 4.13 | 3.22 | 3.18 | 4.64 | 0.12 | 3.68 | 4.87 | 3.71 |
| $K_2O$ | 2.84 | 3.07 | 3.76 | 2.24 | 3.91 | 0.71 | 1.67 | 1.69 |
| $P_2O_5$ | 0.02 | 0.05 | 0.01 | 0.02 | 0.21 | 0.08 | 0.08 | 0.14 |
| $SiO_2/Al_2O_3$ | 6.78 | 6.29 | 6.66 | 6.58 | 3.74 | 9.07 | 6.42 | 6.18 |
| LOI | 0.57 | 0.65 | 0.5 | 1.02 | 18.1 | 2.1 | 2.41 | 3.96 |
| Total | 99.81 | 100.24 | 100.59 | 101.81 | 98.13 | 100.93 | 100.05 | 99.36 |
| Cr | 60 | 110 | 120 | 30 | 680 | 150 | 200 | 110 |
| V | 6 | 5 | <5 | <5 | 93 | 17 | 19 | 15 |
| Ni | 3 | <1 | <1 | <1 | 190 | 7 | 2 | 2 |
| Cs | 0.41 | 1.81 | 0.19 | 0.38 | 3.19 | 0.79 | 0.58 | 1.43 |
| Rb | 55.8 | 64.2 | 61.3 | 40.9 | 104 | 20.2 | 28.4 | 46.3 |
| Ba | 1040 | 1050 | 1205 | 1005 | 534 | 206 | 597 | 573 |
| Th | 4.38 | 3.14 | 4.22 | 5.19 | 1.34 | 2.69 | 3.03 | 3.48 |
| U | 1.62 | 0.85 | 1.62 | 1.65 | 0.57 | 1.33 | 1.12 | 1.33 |
| Nb | 8.6 | 7.1 | 8 | 7.8 | 1.9 | 4.9 | 4.6 | 7.1 |
| Ta | 0.4 | 0.4 | 0.5 | 0.4 | <0.1 | 0.3 | 0.3 | 0.4 |
| La | 15.5 | 19.5 | 30.5 | 29.6 | 9.9 | 17.2 | 18.1 | 21.8 |
| Ce | 36.6 | 44.2 | 67 | 62.7 | 19.7 | 35.4 | 38.5 | 51.6 |
| Pr | 5.84 | 6.16 | 9.47 | 8.79 | 2.72 | 4.77 | 5.3 | 7.64 |
| Sr | 56.4 | 144 | 136 | 59.5 | 979 | 187.5 | 225 | 81.5 |
| Nd | 24.6 | 24.9 | 36.8 | 34.2 | 11 | 18.4 | 20.3 | 30.2 |
| Sm | 6.12 | 6.5 | 9.36 | 7.93 | 2.52 | 4.08 | 4.36 | 7.81 |
| Hf | 8.8 | 7.2 | 9 | 9.5 | 1.6 | 4.1 | 4.4 | 7 |
| Zr | 317 | 254 | 321 | 339 | 56 | 146 | 155 | 250 |
| Eu | 1.13 | 1.44 | 1.6 | 1.7 | 0.8 | 0.7 | 0.97 | 1.74 |
| Gd | 7.07 | 6.98 | 10.3 | 8.74 | 2.69 | 4.11 | 4.59 | 8.55 |
| Tb | 1.24 | 1.19 | 1.63 | 1.46 | 0.35 | 0.62 | 0.68 | 1.36 |
| Dy | 8.42 | 7.81 | 10.25 | 9.08 | 2.07 | 3.87 | 4.11 | 8.28 |
| Ho | 1.78 | 1.56 | 2.03 | 1.85 | 0.37 | 0.75 | 0.8 | 1.71 |
| Er | 5.79 | 5.06 | 6.49 | 6.07 | 1.13 | 2.31 | 2.59 | 5.17 |
| Tm | 0.86 | 0.75 | 0.95 | 0.82 | 0.15 | 0.34 | 0.38 | 0.78 |
| Y | 51 | 44.2 | 58.3 | 52.5 | 10.6 | 21.2 | 23.4 | 48 |
| Yb | 6.25 | 5.16 | 6.54 | 5.87 | 0.93 | 2.43 | 2.7 | 5.47 |
| Lu | 0.9 | 0.74 | 1.01 | 0.9 | 0.15 | 0.36 | 0.43 | 0.8 |
| Sn | 1 | 2 | 3 | 4 | 1 | 1 | 1 | 2 |
| W | <1 | <1 | <1 | <1 | 14 | 10 | 1 | 45 |
| Au | 0.01 | 0.001 | 0.1 | 0.01 | 0.8 | 0.5 | 0.6 | 0.6 |

*Oxides reported in wt-%.
*Gold values reported in g/t.

during alteration and metamorphism. LOI contents are low in the unmineralised schists (LOI = 2.1–4.6 wt. %), except for two samples with high values of 7.8 and 14.4 wt. % (Table 2). The mineralised schists have very high LOI contents of 3.6–9.0 wt. %. These values imply that there is no significant remobilisation of the major elements of the unmineralised schist compared to the mineralised schist which may have experienced some significant remobilisation of their major elements. The remobilisation in the mineralised schists has led to higher concentrations of CaO $Na_2O$, $Fe_2O_3$, and MgO.

The High Field Strength Elements (HFSEs) and the REEs are usually immobile during alteration and metamorphism. The schists and gneisses show a uniformly smooth REE pattern that resembles PAAS and UCC (Figure 8(a,b), Figure 9(a,b)), a feature that would not be expected when the elements are remobilised during metamorphism (McLennan and Taylor 1991; Girty et al. 1994). The covariance of the trace elements demonstrates the chemical consistency and homogeneity of the data and thus suggesting no large-scale remobilisation on these elements.

## Provenance of the schists

### Composition of source rock

During weathering, transportation, and diagenesis, $Al_2O_3$ and $TiO_2$ are not remobilised, thus, their concentration in the resultant rock remains the same as their proto-source rock (Hayashi et al. 1997; Young and Nesbitt 1999). The ratio of $Al_2O_3/TiO_2$ ranges from 3 to 8, 8 to 21, and 21 to 70 for mafic, intermediate, and felsic igneous rocks respectively (Hayashi et al. 1997). The schists were derived from intermediate to felsic proto-source rock having $Al_2O_3/TiO_2$ ratios of 13 and 48 for unmineralised and 11–31 for mineralised (Table 2).

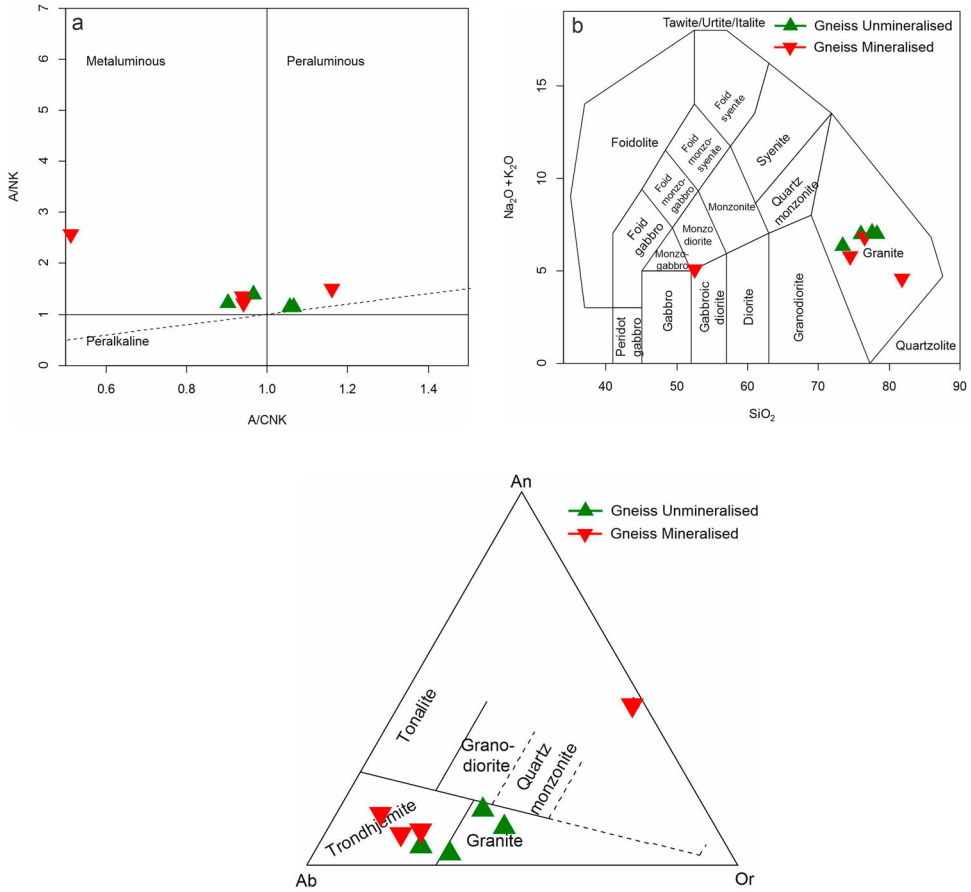


**Figure 7.** (a) A/NK vs A/CNK diagram for the gneisses showing the dominant metaluminous to weak peraluminous nature of the rocks (b) $Na_2O + K_2O$ vs $SiO_2$ diagram for the gneisses classifying the rocks as mostly granite, with one mineralised sample plotting on the boundary line between monzo-diorite and gabbroic diorite. (c) Feldspar discrimination plots after Barker (1979) of the gneisses. Note that the unmineralised gneiss plot mostly as granite with the mineralised gneiss plotting as trondhjemite.

Trace elements, especially, the REEs, Th, and Sc are mostly relied on as useful indicators of provenance and tectonic setting of siliciclasitic rocks (Taylor and McLennan 1985). This is because post-depositional processes, e.g. diagenesis and metamorphism do not influence the abundance of these elements (McLennan and Taylor 1991; Condie 1993). The composition of the source rock from which the sediments formed and accumulated into the basin manifests in the siliciclastic rock's REE patterns. In general, the REE patterns do not vary significantly when the sediments are derived from a common source. On the other hand, wide variations are shown in REE patterns when the sediments are derived from mixed sources (Nance and Taylor 1977; Taylor and McLennan 1985; Cullers 1995). The schists show smooth REE patterns with no significant variations, evidence of probably a common sediment source area (s) (Figure 9(a,b)).

Mafic igneous rocks usually have low and/or no negative Eu anomaly (Eu/Eu* = 0.8–1), yet high negative Eu anomaly (Eu/Eu* = 0.5–0.8) are often observed in felsic igneous rocks (Taylor and McLennan 1985; Cullers 1994; Cullers and Podkovyrov 2002). The schists of the study area all show significant negative Eu anomalies (0.47–0.84 for the unmineralised and 0.62–0.95 for the mineralised, Table 3). In view of that, the provenance of the schists is explained as dominated by detritus derived from intermediate and felsic proto-source rocks.

To further assess the composition of the schists, the ratios of $(La/Lu)_N$, Th/Sc, and La/Sc were employed (Table 3). These trace element ratios provide information about the composition of the source rock because Th, La, and Lu are incompatible elements, enriched in felsic rocks, while Sc is a compatible element, enriched in mafic rocks (Cullers 1994, 2000). The trace element ratios of the schists, suggest they were derived from a combination of felsic and intermediate rocks (Table 3). The composition of the source rock of the schists is inferred in the La/Th vs. Hf discrimination diagram (Floyd and Leveridge 1987). The schists plot in the field of the mixed felsic and mafic sources, and andesitic source (Figure10). Overall, the schists were derived from mixed sources of felsic and intermediate source rocks.

### *Petrogenesis of the granitoid gneisses*

The gneisses of the study area have dominantly metaluminous to weakly peraluminous characteristics,

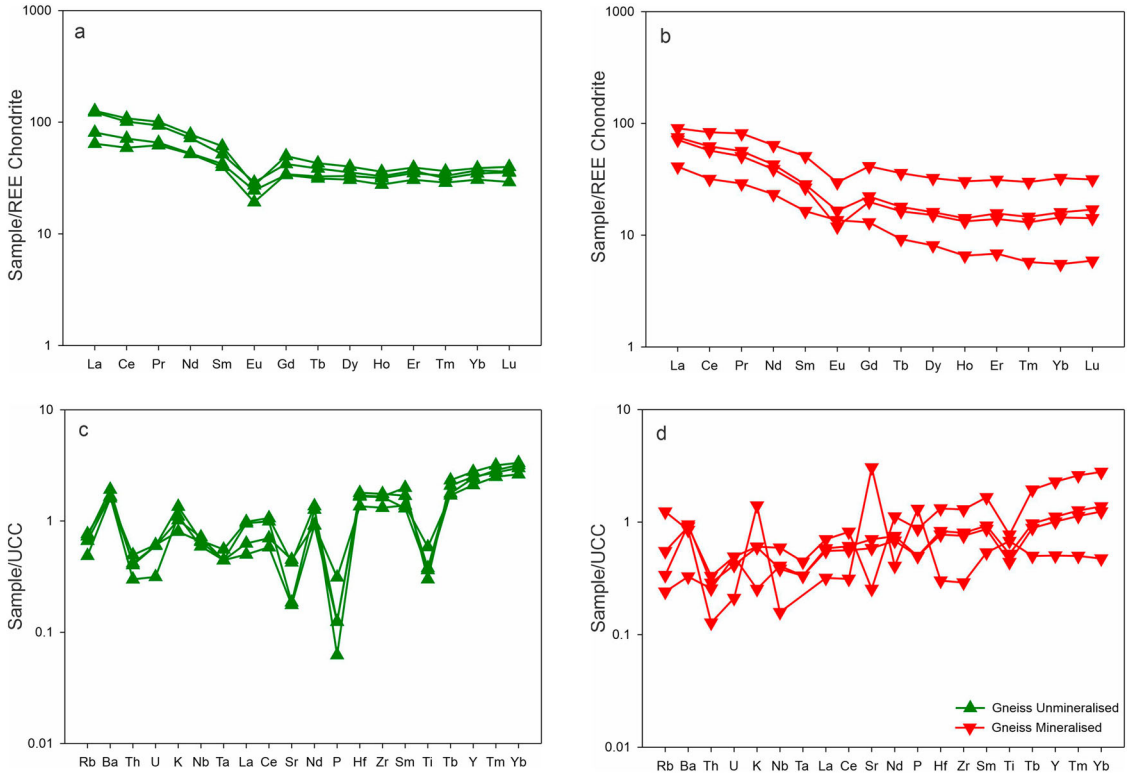


**Figure 8.** (a) Sample normalised to REE chondrite diagram for unmineralised gneiss. The samples show a relatively enriched LREE and nearly flat HREE pattern. (b) Sample normalised to REE chondrite diagram for mineralised gneiss. Though the pattern appears similar to the unmineralised gneiss, these samples show a widespread concentration than the unmineralised gneiss. (c) Spider diagram for unmineralised gneiss. Note the negative Nb-Ta and Ti peak. (d) Spider diagram for mineralised gneiss. Note: the mineralised gneiss shows a wide-spread trace element concentration than the unmineralised gneiss.

contain moderate to high total alkalis ($Na_2O + K_2O$ = 2.71–8.38 wt-%), which are features usually associated with I-type granitoids, and the chemical composition suggests that they are products by partial melting of a mafic mantle-derived igneous source material (probably of a sub-crustal underplate, but subducted-slab crust or older high-level pluton sources cannot be excluded) (Barbarin 1990; 1999). The occurrence of biotite-hornblende and biotite-bearing gneiss rocks within the study area, and the absence of two-mica granitoids also rules out sediment contribution in the Abansuoso area (Grenholm 2011). The gneisses on the multi-element diagrams normalised to UCC show high HREE fractionation (Figure 8(c,d)). According to Grenholm (2011), the high degree of HREE-fractionation observed in some granitoids in the Birimian terrain of the WAC can be linked to the stability of garnet in the residue hence implying deeper crustal levels even though fractionation of HREEs may also be the result of residual accessory phases such as zircon. The trace element characteristics of the gneisses are akin to I-type rocks, and thus can be interpreted as derivatives from mafic igneous precursor (thickened mafic lower crust), generated in convergent margins (Liu et al. 2019; Sakyi et al. 2020).

## *Tectonic settings of the schists and gneiss*

The characteristic Nb-Ta trough and negative P and Ti peaks displayed by the schists and gneisses on the multi-elements normalised to UCC diagrams is an indication of their formation in an arc environment. The tectonic setting of the rocks of the Abansuoso area is identified by using different discriminant diagram. $DF_{(A\text{-}P)M}$ indicates that the majority of the schist rocks in the study area were emplaced in an active continental margin (Figure 11(a)). To further constrain the tectonic setting of the schist, the Th – Sc – Zr/10 discrimination diagram was plotted (Bhatia and Crook 1986) to distinguish among Passive Margin (PM), Active Continental Margin (ACM), Continental arc (CA), and Island Arc (IA) settings. The Th – Sc – Zr/10 plot (Figure 11(b)) places the schist in and around the continental arc setting. The gneisses plot within the active continental margin and VAG + syn-collisional granites field on the Th/Ta vrs Yb and Y vrs Nb diagrams, respectively (Figure 12(a,b)). All these support the fact that the gneisses and schists were formed in an arc environment. Thus they are orogenic rather than anorogenic in nature.

**Table 2.** Major and trace elements composition of the schists.

| | Unmineralised schist | | | | | | | | Mineralised schist | | | | | | |
|---|---|---|---|---|---|---|---|---|---|---|---|---|---|---|---|
| Sample | 002/81 | 004/81 | 001/81 | 003/81 | 008/81 | 001/OS | 008/PK | OS/A | 009/81 | 012/79 | 019/79 | 011/79 | 013/79 | 014/79 | 020/79 |
| $SiO_2$ | 49.9 | 56.5 | 60.4 | 54.3 | 61.5 | 75.7 | 79.5 | 76.9 | 74.9 | 74.4 | 74.4 | 64.9 | 65.2 | 67.1 | 72 |
| $TiO_2$ | 0.65 | 0.95 | 0.67 | 1.18 | 0.49 | 0.22 | 0.26 | 0.25 | 0.45 | 0.51 | 0.58 | 0.66 | 0.64 | 0.68 | 0.53 |
| $Al_2O_3$ | 10.35 | 12.1 | 9.6 | 12.6 | 14.95 | 10.55 | 12.2 | 11.15 | 9.38 | 10.7 | 10.65 | 10.6 | 12.1 | 11.75 | 10.05 |
| FeOt | 8.02 | 9.46 | 7.49 | 11.15 | 2.8 | 2.49 | 1.4 | 2.39 | 4.87 | 4.49 | 5.92 | 6.68 | 6.92 | 7.54 | 7.91 |
| MnO | 0.16 | 0.13 | 0.13 | 0.19 | 0.12 | 0.06 | <0.01 | 0.05 | 0.13 | 0.12 | 0.06 | 0.23 | 0.16 | 0.15 | 0.02 |
| MgO | 5.1 | 2.11 | 2.33 | 2.8 | 1.44 | 0.5 | 0.2 | 0.44 | 0.61 | 0.4 | 0.2 | 0.99 | 0.57 | 0.92 | 0.24 |
| CaO | 7.7 | 4.8 | 4.83 | 4.54 | 3.86 | 1.56 | 0.03 | 1.31 | 1.66 | 1.27 | 0.56 | 3.81 | 2.19 | 2.29 | 0.54 |
| $Na_2O$ | 2 | 4.46 | 3.96 | 5.07 | 7.45 | 2.85 | 0.12 | 3.06 | 2.03 | 3.55 | 4.13 | 1.73 | 3.89 | 4.04 | 0.31 |
| $K_2O$ | 1.96 | 1.4 | 0.99 | 0.78 | 1 | 1.86 | 3.79 | 1.91 | 1.93 | 1.49 | 1.14 | 2.4 | 1.74 | 2.18 | 3.06 |
| $P_2O_5$ | 0.1 | 0.22 | 0.08 | 0.23 | 0.01 | 0.08 | 0.02 | 0.1 | 0.14 | 0.22 | 0.24 | 0.19 | 0.3 | 0.2 | 0.15 |
| $SiO_2/Al_2O_3$ | 4.82 | 4.67 | 6.29 | 4.31 | 4.11 | 7.18 | 6.52 | 6.9 | 7.99 | 6.95 | 6.99 | 6.12 | 5.39 | 5.71 | 7.16 |
| LOI | 14.35 | 7.77 | 8.96 | 7.45 | 6.02 | 2.93 | 2.07 | 2.75 | 4.6 | 3.82 | 2.29 | 8.19 | 6.26 | 3.83 | 5.28 |
| Total | 100.4 | 100.01 | 99.5 | 100.38 | 99.73 | 98.9 | 99.69 | 100.4 | 100.76 | 101.05 | 100.21 | 100.58 | 100.06 | 100.8 | 100.19 |
| Cr | 430 | 120 | 170 | 60 | 70 | 140 | 140 | 200 | 190 | 190 | 180 | 160 | 170 | 180 | 140 |
| V | 249 | 244 | 150 | 302 | 32 | 19 | 10 | 27 | 16 | 23 | 21 | 68 | 25 | 19 | 33 |
| Ni | 38 | 4 | 6 | 4 | 6 | 3 | 1 | 4 | 1 | 3 | 4 | <1 | 1 | <1 | 4 |
| Cs | 2.14 | 1.72 | 0.96 | 1.02 | 0.5 | 1.17 | 1.1 | 1.13 | 0.9 | 0.91 | 0.57 | 1.42 | 0.97 | 1.11 | 1.64 |
| Ba | 304 | 733 | 158.5 | 443 | 342 | 591 | 748 | 583 | 303 | 525 | 216 | 1430 | 527 | 796 | 732 |
| Rb | 56.2 | 34.4 | 26.1 | 22 | 21.6 | 42.1 | 79.5 | 42.8 | 41.4 | 34.7 | 24.9 | 48.9 | 36.6 | 45 | 67.6 |
| Th | 0.66 | 1.14 | 0.69 | 1.32 | 3.37 | 3.54 | 4.05 | 3.99 | 2.5 | 3.11 | 3.13 | 3.72 | 3.42 | 2.99 | 3.2 |
| U | 0.25 | 0.54 | 0.3 | 0.57 | 0.93 | 1.21 | 1.62 | 1.13 | 1.02 | 1.22 | 1.14 | 1.19 | 1.54 | 1.17 | 1.31 |
| Nb | 2.7 | 2.5 | 1.7 | 3 | 6.7 | 5.1 | 7.7 | 7.4 | 5.3 | 5.7 | 5.7 | 7.6 | 7.3 | 6.3 | 5.9 |
| Ta | 0.1 | 0.1 | <0.1 | 0.1 | 0.5 | 0.4 | 0.5 | 0.4 | 0.3 | 0.3 | 0.4 | 0.5 | 0.4 | 0.4 | 0.4 |
| La | 6.9 | 11.2 | 5.8 | 11.2 | 21.7 | 23.5 | 28.5 | 25.8 | 18.9 | 24.2 | 23.8 | 27.1 | 27.1 | 23.6 | 24.4 |
| Ce | 15.8 | 22.4 | 12.6 | 23.1 | 44.6 | 47.4 | 56.5 | 53.8 | 38.9 | 49.7 | 50.5 | 57.9 | 56.7 | 50.3 | 52.5 |
| Pr | 2.44 | 3.26 | 1.91 | 3.47 | 6.29 | 6.54 | 8.2 | 7.38 | 5.69 | 7.25 | 7.2 | 8.32 | 8.3 | 7.27 | 7.53 |
| Sr | 259 | 264 | 225 | 280 | 378 | 117 | 9.1 | 102.5 | 93.8 | 92.5 | 82.1 | 266 | 161.5 | 208 | 38.3 |
| Nd | 10 | 13.4 | 7.7 | 14.4 | 24.2 | 24.7 | 32.7 | 28.1 | 23.5 | 28.6 | 28.2 | 33.3 | 33.4 | 29.8 | 30.6 |
| Sm | 2.46 | 3.47 | 2.21 | 3.89 | 6.15 | 5.82 | 8.38 | 6.61 | 6.6 | 7.52 | 7.41 | 8.72 | 9.1 | 7.7 | 7.51 |
| Hf | 1.3 | 2.2 | 1.5 | 2.7 | 5.8 | 6.2 | 8.5 | 6.8 | 4.9 | 5.6 | 6.6 | 7.4 | 7 | 6.1 | 5.9 |
| Zr | 48 | 83 | 51 | 93 | 196 | 217 | 310 | 243 | 176 | 198 | 227 | 260 | 251 | 215 | 214 |
| Eu | 0.67 | 0.99 | 0.61 | 1.25 | 1.32 | 0.91 | 1.65 | 1.08 | 1.52 | 1.77 | 1.75 | 2.04 | 2.31 | 1.82 | 1.62 |
| Gd | 2.32 | 4.12 | 2.38 | 4.21 | 6.87 | 5.96 | 9.54 | 6.86 | 7.25 | 7.79 | 8.47 | 9.27 | 10.5 | 8.54 | 7.82 |
| Tb | 0.35 | 0.62 | 0.38 | 0.65 | 1.14 | 0.9 | 1.57 | 1.07 | 1.17 | 1.24 | 1.34 | 1.49 | 1.68 | 1.32 | 1.2 |
| Dy | 2.02 | 3.91 | 2.25 | 4.05 | 7.21 | 5.71 | 10.25 | 6.49 | 7.21 | 6.97 | 8.43 | 9.36 | 10.8 | 8.15 | 7.12 |
| Ho | 0.41 | 0.78 | 0.44 | 0.81 | 1.47 | 1.14 | 2.1 | 1.27 | 1.45 | 1.41 | 1.77 | 1.88 | 2.19 | 1.6 | 1.42 |
| Er | 1.19 | 2.41 | 1.33 | 2.42 | 4.55 | 3.67 | 6.66 | 4.3 | 4.48 | 4.34 | 5.48 | 6.11 | 6.52 | 5.06 | 4.28 |
| Tm | 0.17 | 0.35 | 0.19 | 0.34 | 0.67 | 0.56 | 0.93 | 0.65 | 0.63 | 0.63 | 0.79 | 0.92 | 0.89 | 0.71 | 0.64 |
| Y | 11.5 | 22.2 | 12.6 | 22.7 | 44 | 33.1 | 61.7 | 38 | 41.6 | 39.1 | 49 | 55.2 | 62.7 | 46.3 | 41.1 |
| Yb | 1.14 | 2.28 | 1.41 | 2.3 | 4.52 | 3.78 | 6.57 | 4.62 | 4.24 | 4.28 | 5.38 | 6.33 | 6.15 | 5 | 4.32 |
| Lu | 0.16 | 0.32 | 0.21 | 0.35 | 0.63 | 0.57 | 0.94 | 0.69 | 0.62 | 0.65 | 0.74 | 0.96 | 0.87 | 0.71 | 0.65 |
| Sn | <1 | 1 | <1 | 1 | 1 | 1 | 2 | 2 | 1 | 1 | 1 | 3 | 2 | 1 | 3 |
| W | 3 | <1 | 8 | 2 | 8 | 12 | 18 | 14 | 36 | 48 | 46 | 55 | 72 | 3 | 40 |
| Au | 0.03 | 0.01 | 0.22 | 0.01 | 0.01 | 0.01 | 0.11 | 0.11 | 2.1 | 0.9 | 2 | 1.4 | 1.04 | 0.5 | 1.66 |

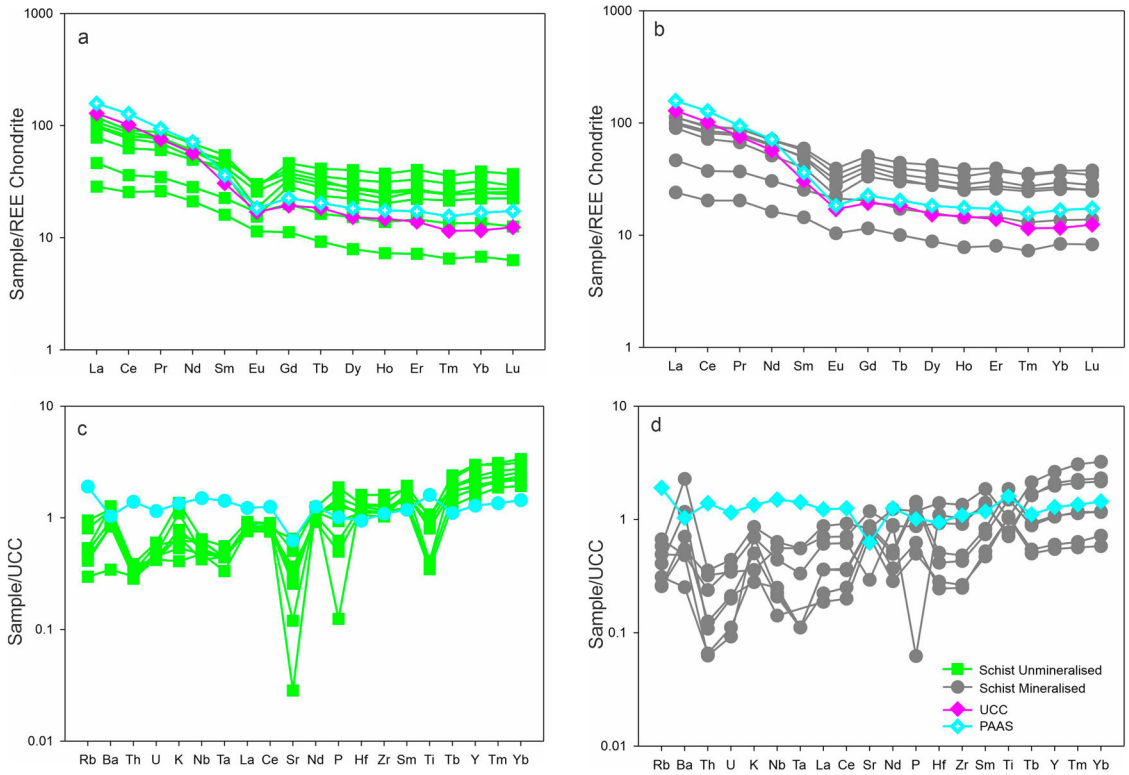


**Figure 9.** (a) Sample normalised to REE chondrite diagram for unmineralised schist. The samples show a relatively enriched LREE and nearly flat HREE pattern similar to the unmineralised gneiss. (b) Sample normalised to REE chondrite diagram for mineralised schist. Though the pattern appears similar to the unmineralised gneiss, these samples show a widespread concentration than the unmineralised schist. (c) Spider diagram for unmineralised schist showing typical Nb-Ta and Ti negative peaks similar to arc-derived rocks. (d) Spider diagram for mineralised schist howing typical Nb-Ta and Ti negative peaks similar to arc-derived rocks.

## *Geodynamic implication and the type of ore deposit*

Major and trace element concentrations of schist from the Abansuoso area of the Sefwi greenstone belt indicate that they originated from a mixed source of intermediate to felsic continental basement rocks. Since these schists have similar trace element patterns as the gneisses, this could connote their derivation from a similar proto source as the gneisses. The gneisses are dominantly granite (unmineralised) and trondhjemite (mineralised) and the schists may have been sourced from similar rocks. One key observation made from this study is the fact that although on average, the major and trace element composition of the mineralised schists and gneisses are significantly different from that of the unmineralised varieties, they plot in a similar field on provenance/petrogenetic and tectonic setting discrimination diagrams. Therefore, the mineralisation process(es) have had little effect on the source characteristics of the mineralised rocks. This study has therefore revealed that in regions where rocks have been significantly obliterated by the mineralisation process, a comparative study of the mineralised and unmineralised rocks can be used to constrain the source and geodynamic evolution of the mineralised rocks, according to the findings of this study.

The Birimian terrain has over the years been proposed to represent a juvenile arc crust formed during the Rhyacian Eburnean orogeny (Dampare et al. 2008; Baratoux et al. 2011; Senyah et al. 2016). It is widely accepted that the rocks of the Birimian terrain formed in a suprasubduction zone, arc-back-arc basin, or accretion of several oceanic arc terrains (Dampare et al. 2008; Sakyi et al. 2018; McFarlane et al. 2019). In this study, the gneisses and the schists were formed in an arc environment, probably syn-orogenic. This assertion is supported by Abitty et al. (2015) and Senyah et al. (2016) who made similar findings in the Northern and Southwestern part of Ghana respectively. Volcanic arc granites are associated with magma sources depleted in mantle material which has crustal components through the subduction process (Pearce 1996). Thus, the gneisses and schist may have formed during the subduction accretion processes during the Rhyacian Eburnean orogeny as has been proposed by many authors. This finding may

**Table 3.** Elemental ratios of the schists compared with sediments derived from felsic and mafic rocks.

| | Mineralised | Unmineralised | Range of sediments from felsic sources | Range of sediments from mafic sources |
|---|---|---|---|---|
| La/Sc | 0.22–2.02 | 1.57–9.50 | 2.50–16.3 | 0.43–0.86 |
| Th/Sc | 0.02–0.31 | 0.20–1.35 | 0.84–20.5 | 0.05–0.22 |
| Eu/Eu* | 0.62–0.94 | 0.47–0.85 | 0.40–0.94 | 0.71–0.95 |
| (La/Lu)N | 2.91–3.95 | 3.19–4.54 | 3.00–27.0 | 1.10–7.00 |

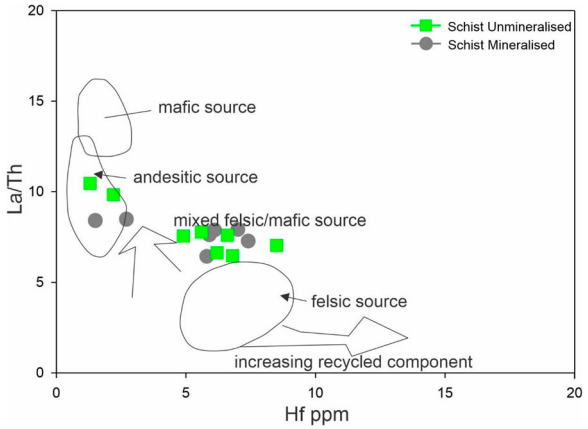


**Figure 10.** Plot of La/Th against Hf for the schist (composition fields after Floyd and Leveridge 1987). The samples generally show felsic to intermediate source rock composition plotting in the field of andesite and mixed felsic/mafic sources.

suggest that the mineralisation in the gneisses and schists is a typical orogenic type of mineralisation. Intrusion-related and orogenic gold deposits share a number of characteristics (Groves et al. 1998).

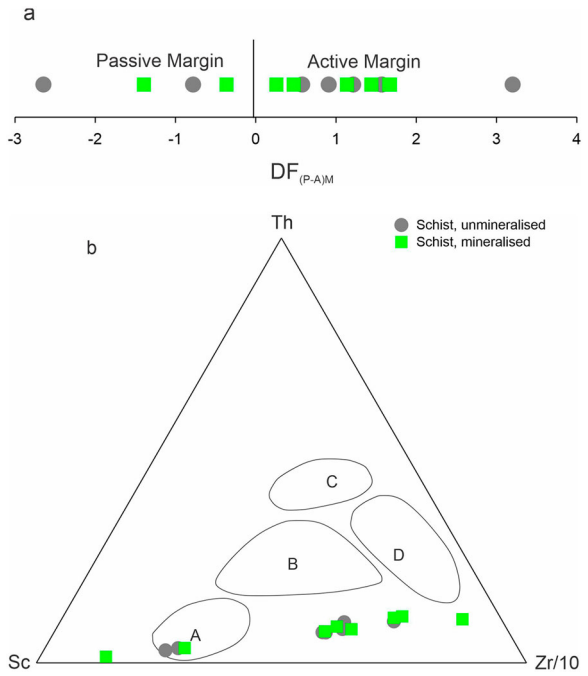


**Figure 11.** (a) Tectonic setting discrimination diagrams for the schists $DF_{(A\text{-}P)M}$ (Verma and Armstrong-Altrin, 2016). The samples plot dominantly in the active margin setting. (b) Tectonic setting discrimination diagrams for the schists Th – Co – Zr/10 plot (Bhatia and Crook 1986). DF = Discriminant function, A and P are active and passive margin respectively, and M = major element composition.

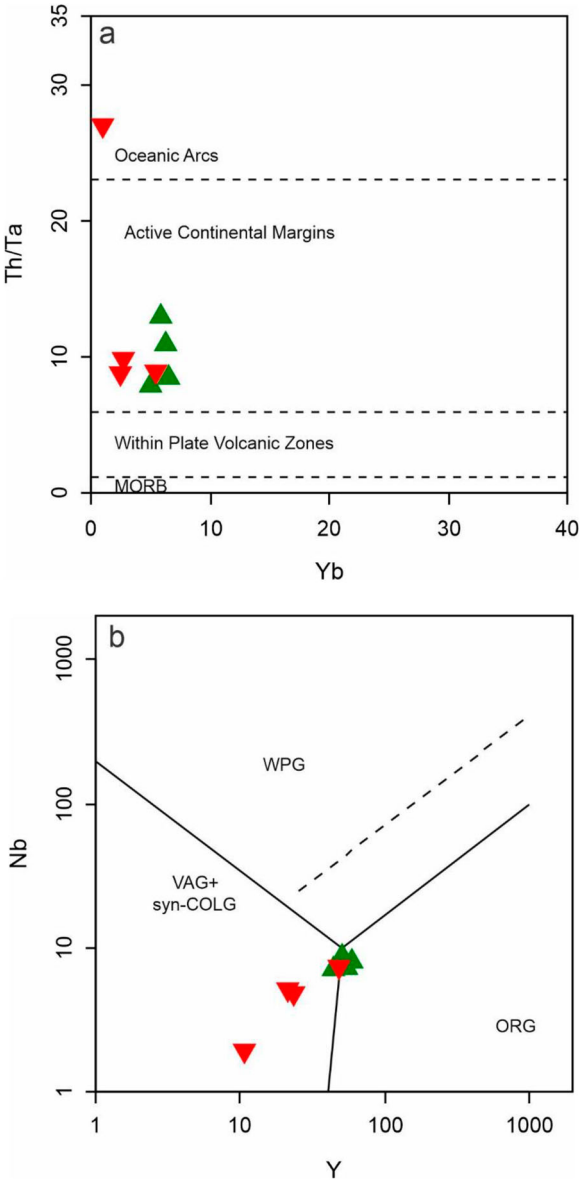


**Figure 12.** (a) Tectonic setting discrimination diagrams for the gneiss using Th/Ta vs Yb. The gneisses plot mainly in the active margin, an indication of their derivation from an active (arc) setting. (b). Nb vs Y tectonic setting discrimination diagrams for the gneiss showing that the gneisses were probably derived from a volcanic-arc and syn-collisional setting.

Despite their similarities, orogenic gold deposits are related to metamorphic rocks with an amphibolite-facies and/or greenschist composition, and magmatic intrusions (Phillips and Powell 2009; Goldfarb and Groves 2015). In this study, the gneisses and schists have mineral assemblage typical of greenschist and lower amphibolite facies, supporting the orogenic origin of gold mineralisation.

## Conclusion

Major and trace element compositions have been used to infer the mode and environment of formation of the mineralised and unmineralised gneisses and schists from the Abansuoso deposit within the Sefwi greenstone belt. On the chondrite normalised REE diagram, both the mineralised and unmineralised gneisses display enriched LREE and nearly flat HREE patterns similar to the schists. The multi-elements normalised to UCC diagrams show that the gneisses and schists have depleted concentration of LILE and enriched contents of HFSE including the HREE, with typical Nb-Ta trough. The schists from their major and trace element composition were deposited in an active continental margin, perhaps a continental arc setting. A similar continental arc setting has been inferred for the gneisses from their tectonic setting discrimination diagrams and trace patterns, with typical Nb-Ta trough. This study has revealed that a comparative study of the major and trace element composition of the mineralised and unmineralised rocks from an area is useful in constraining the source and geodynamic evolution of the mineralised rocks.

## Acknowledgements

This research paper is part of the first author's PhD work, and he is thankful to the African Union and Pan African University for the award of this PhD. Scholarship. The first author is also grateful to the University for Development Studies for granting his study leave. The first author is very grateful to Supercare Gold and Pelangio Exploration Company for granting him access to their concession and providing him with the needed assistance for the fieldwork. The authors are also thankful to Prof. Neil Philips and an anonymous reviewer for their helpful comments, suggestions, and thoughtful reviews which have greatly enhanced the quality of this paper.

## Disclosure statement

No potential conflict of interest was reported by the author (s).

## ORCID

*Raymond Webrah Kazapoe* http://orcid.org/0000-0002-0307-7834

## References

Abitty EK, Dampare SB, Nude PM, Asiedu DK. 2016. Geochemistry and petrogenesis of the K-rich 'Bongo-type'granitoids in the Paleoproterozoic Bole–Nangodi greenstone belt of Ghana. J Afr Earth Sci. 122:47–62.

Agbenyezi TK, Foli G, Gawu SK. 2020. Geochemical characteristics of gold-bearing Granitoids at Ayanfuri in the Kumasi Basin, Southwestern Ghana: implications for the orogenic related gold systems. Earth Sci Malaysia (ESMY). 4(2):127–134.

Allibone A, Hayden P, Cameron G, Duku F. 2004. Paleoproterozoic gold deposits hosted by albite-and carbonate-altered tonalite in the Chirano District, Ghana, West Africa. Econ Geol. 99(3):479–497.

Amponsah PO, Salvi S, Didier B, Baratoux L, Siebenaller L, Jessell M, Nude PM, Gyawu EA. 2016. Multistage gold mineralization in the Wa-Lawra greenstone belt, NW Ghana: The Bepkong deposit. J Afr Earth Sci. 120:220–237.

Baratoux L, Metelka V, Naba S, Jessell MW, Grégoire M, Ganne J. 2011. Juvenile Paleoproterozoic crust evolution during the Eburnean orogeny (~ 2.2-2.0 Ga), western Burkina Faso. Precambrian Res. 191(1–2):18–45.

Barbarin B. 1990. Granitoids: main petrogenetic classifications in relation to origin and tectonic setting. Geol J. 25(3–4):227–238.

Barbarin B. 1999. A review of the relationships between granitoid types, their origins and their geodynamic environments. Lithos. 46(3):605–626.

Barker F. 1979. Trondhjemite: definition, environment and hypotheses of origin. In: Developments in petrology, Vol. 6. Amsterdam (Netherlands): Elsevier; p. 1–12.

Bhatia MR, Crook KA. 1986. Trace element characteristics of graywackes and tectonic setting discrimination of sedimentary basins. Contrib Mineral Petrol. 92(2):181–193.

Bouabdellah M, Slack JF. 2016. Geologic and metallogenic framework of North Africa. In: Slack J, editor. Mineral deposits of North Africa. Cham: Springer; p. 3–81.

Condie KC. 1993. Chemical composition and evolution of the upper continental crust: contrasting results from surface samples and shales. Chem Geol. 104(1–4):1–37.

Cullers RL. 1994. The controls on the major and trace element variation of shales, siltstones, and sandstones of Pennsylvanian-Permian age from uplifted continental blocks in Colorado to platform sediment in Kansas, USA. Geochim Cosmochim Acta. 58(22):4955–4972.

Cullers RL. 1995. The controls on the major-and trace-element evolution of shales, siltstones and sandstones of Ordovician to Tertiary age in the wet Mountains region, Colorado, USA. Chem Geol. 123(1–4):107–131.

Cullers RL. 2000. The geochemistry of shales, siltstones and sandstones of Pennsylvanian–Permian age, Colorado, USA: implications for provenance and metamorphic studies. Lithos. 51(3):181–203.

Cullers RL, Podkovyrov VN. 2002. The source and origin of terrigenous sedimentary rocks in the Mesoproterozoic Ui group, south-eastern Russia. Precambrian Res. 117(3–4):157–183.

Dampare SB, Shibata T, Asiedu DK, Osae S, Banoeng-Yakubo B. 2008. Geochemistry of Paleoproterozoic metavolcanic rocks from the southern Ashanti volcanic belt, Ghana: petrogenetic and tectonic setting implications. Precambrian Res. 162(3–4):403–423.

Floyd PA, Leveridge BE. 1987. Tectonic environment of the Devonian Gramscatho basin, south Cornwall: framework mode and geochemical evidence from turbiditic sandstones. J Geol Soc London. 144(4):531–542.

Fougerouse D, Micklethwaite S, Ulrich S, Miller J, Godel B, Adams DT, McCuaig TC. 2017. Evidence for two stages of mineralization in West Africa's largest gold deposit: Obuasi, Ghana. Econ Geol. 112(1):3–22.

Galipp K, Klemd R, Hirdes W. 2003. Metamorphism and geochemistry of the paleoproterozoic Birimian sefwi volcanic belt (Ghana, West Africa). Geologisches Jahrbuch D. 111:151–191.

Girty GH, Hanson AD, Knaack C, Johnson D. 1994. Provenance determined by REE, Th, and Sc analyses of

metasedimentary rocks, Boyden Cave roof pendant, central Sierra Nevada, California. J Sediment Res. 64(1b):68–73.
Goldfarb RJ, Baker T, Dubé B, Groves DI, Hart CJ, Gosselin P. 2005. Distribution, character, and genesis of gold deposits in metamorphic terrain.
Goldfarb RJ, Groves DI. 2015. Orogenic gold: common or evolving fluid and metal sources through time. Lithos. 233:2–26.
Goldfarb RJ, Groves DI, Gardoll S. 2001. Orogenic gold and geologic time: a global synthesis. Ore Geol Rev. 18(1–2):1–75.
Grenholm M. 2011. Petrology of Birimian granitoids in southern Ghana: petrography and petrogenesis Dissertations in Geology at Lund University, Lund, Sweden.
Griffis J, Barning K, Agezo FL, Akosa F. 2002. Gold deposits of Ghana prepared on behalf of Ghana mineral commission. Ghana: Accra. 432.
Griffis RJ, Agezo FL. 2000. Mineral occurrence and exploration potential of northern Ghana. Mineral Commission Report. 132–1133, Accra.
Groves DI, Goldfarb RJ, Gebre-Mariam M, Hagemann SG, Robert F. 1998. Orogenic gold deposits: a proposed classification in the context of their crustal distribution and relationship to other gold deposit types. Ore Geol Rev. 13(1–5):7–27.
Groves DI, Goldfarb RJ, Robert F, Hart CJ. 2003. Gold deposits in metamorphic belts: overview of current understanding, outstanding problems, future research, and exploration significance. Econ Geol. 98(1):1–29.
Hart CJ, Goldfarb RJ, Qiu Y, Snee L, Miller LD, Miller ML. 2002. Gold deposits of the northern margin of the North China Craton: multiple late Paleozoic–Mesozoic mineralizing events. Miner Deposita. 37 (3):326–351.
Hayashi KI, Fujisawa H, Holland HD, Ohmoto H. 1997. Geochemistry of~ 1.9 Ga sedimentary rocks from northeastern Labrador, Canada. Geochim Cosmochim Acta. 61 (19):4115–4137.
Jessell MW, Amponsah PO, Baratoux L, Asiedu DK, Loh GK, Ganne J. 2012. Crustal-scale transcurrent shearing in the paleoproterozoic Sefwi-Sunyani-Comoe region, West Africa. Precambrian Res. 212:155–168.
Kazapoe RW, Olugbenga O, Arhin E, Olisa O. 2021. Isotope geochemistry as a tool in the exploration of gold occurrences in Ghana: a review. Arab J Geosci. 14 (19):1–15.
Kazapoe WR, Okunlola O, Arhin E, Olisa O, Harris C, Kwayisi D, Torkonoo S, Amuah EEY. 2022. Geology and isotope systematics of gold deposits in Abansuoso area of Sefwi Belt, Southwestern Ghana. Geol Ecol Landscapes. 6:1–22.
Kempe U, Belyatsky B, Krymsky R, Kremenetsky A, Ivanov P. 2001. Sm–Nd and Sr isotope systematics of scheelite from the giant Au (–W) deposit Muruntau (Uzbekistan): implications for the age and sources of Au mineralization. Miner Deposita. 36(5):379–392.
Liu Y, Chakhmouradian AR, Hou Z, Song W, Kynický J. 2019. Development of REE mineralization in the giant Maoniuping deposit (Sichuan, China): insights from mineralogy, fluid inclusions, and trace-element geochemistry. Miner Deposita. 54(5):701–718.
McFarlane HB, Ailleres L, Betts P, Ganne J, Baratoux L, Jessell MW, Block S. 2019. Episodic collisional orogenesis and lower crust exhumation during the Palaeoproterozoic Eburnean Orogeny: evidence from the Sefwi Greenstone Belt, West African Craton. Precambrian Res. 325:88–110.
McLennan SM, Taylor SR. 1991. Sedimentary rocks and crustal evolution: tectonic setting and secular trends. J Geol. 99(1):1–21.
Nance WB, Taylor SR. 1977. Rare earth element patterns and crustal evolution – II. Archean sedimentary rocks from Kalgoorlie, Australia. Geochim Cosmochim Acta. 41(2):225–231.
Oberthür T, Vetter U, Davis DW, Amanor JA. 1998. Age constraints on gold mineralization and Paleoproterozoic crustal evolution in the Ashanti belt of southern Ghana. Precambrian Res. 89(3–4):129–143.
Pearce JA. 1996. A user's guide to basalt discrimination diagrams. Trace element geochemistry of volcanic rocks: applications for massive sulphide exploration. Geological Association of Canada, Short Course Notes, 12, 79–113.
Perrouty S, Aillères L, Jessell MW, Baratoux L, Bourassa Y, Crawford B. 2012. Revised eburnean geodynamic evolution of the gold-rich southern Ashanti Belt, Ghana, with new field and geophysical evidence of pre-Tarkwaian deformations. Precambrian Res. 204:12–39.
Phillips GN, Powell R. 2009. Formation of gold deposits: review and evaluation of the continuum model. Earth Sci Rev. 94(1–4):1–21.
Sakyi PA, Addae RA, Su BX, Dampare SB, Abitty E, Su BC, Liu B, Asiedu DK. 2020. Petrology and geochemistry of TTG and K-rich Paleoproterozoic Birimian granitoids of the West African Craton (Ghana): petrogenesis and tectonic implications. Precambrian Res. 336:105492.
Sakyi PA, Anum S, Su BX, Nude PM, Su BC, Asiedu DK, Kwayisi D. 2018. Geochemical and Sr-Nd isotopic records of Paleoproterozoic metavolcanics and mafic intrusive rocks from the West African Craton: evidence for petrogenesis and tectonic setting. Geol J. 53(2):725–741.
Schiano P, Dupré B, Lewin E. 1993. Application of element concentration variability to the study of basalt alteration (Fangataufa atoll, French Polynesia). Chem Geol. 104 (1–4):99–124.
Senyah GA, Dampare SB, Asiedu DK. 2016. Geochemistry and tectonic setting of the Paleoproterozoic metavolcanic rocks from the Chirano Gold District, Sefwi belt, Ghana. J Afr Earth Sci. 122:32–46.
Shand SJ. 1948. Eruptive rocks: their genesis, composition, classification, and their relation to ore deposits, with a chapter on meteorites. J Geol. 56(6):593–593.
Sillitoe RH. 1991. Intrusion-related gold deposits. In: Foster RP, editor. Gold metallogeny and exploration. Boston (MA): Springer; p. 165–209.
Smith AJ, Henry G, Frost-Killian S. 2016. A review of the Birimian Supergroup-and Tarkwaian group-hosted gold deposits of Ghana. Episodes. 39(2):177–197.
Takyi-Kyeremeh K, Wemegah DD, Preko K, Menyeh A. 2019. Integrated geophysical study of the Subika Gold Deposit in the Sefwi Belt. Ghana. Cogent Geosci. 5 (1):1585406.
Taylor SR, McLennan SM. 1985. The continental crust: its composition and evolution. Oxford: Blackwell Scientific Publications.

Verma SP, Armstrong-Altrin JS. 2016. Geochemical discrimination of siliciclastic sediments from active and passive margin settings. Sediment Geol. 332:1–12.

Whitney DL, Evans BW. 2010. Abbreviations for names of rock-forming minerals. Am Mineral. 95(1):185–187.

Young GM, Wayne Nesbitt H. 1999. Paleoclimatology and provenance of the glaciogenic Gowganda Formation (Paleoproterozoic), Ontario, Canada: A chemostratigraphic approach. Geol Soc Am Bull. 111 (2):264–274.